Chapter 7:

Enhancing the Effective Bandwidth of a Membrane Optic using a Shallow, Fluid-filled Cavity

7.1 Introduction

One of the fundamental challenges facing the development of membrane optics is the same trait membrane mirror designers are trying to take advantage of: their extreme flexibility. A membrane's low mass, minimal structural rigidity, and negligible damping leads to undesirable system dynamics with sharp response peaks within the frequency bandwidths of interest. To avoid these destructive resonances, the membrane could be pre-stressed to extreme levels, consequently shifting the system resonant frequencies to greater values and increasing the effective bandwidth of the mirror or aperture. However, high levels of pre-stress within the membrane have two undesirable consequences. Firstly, the high tensile loading will make the taut surface rather inflexible, which means the membrane cannot be used as a secondary, deformable mirror in an adaptive optic scheme. As we will show in the next chapter, the inherent flexibility of the membrane is a great asset and can be used advantageously in deformable mirror designs. Secondly, from a mechanical design perspective, the high level of pre-stress also means that the membrane will be subject to fatigue and could easily rupture during operation on-orbit. These issues illuminate a conflict of interest in the use of membranes as mirrors: the optimal design should be lightweight and flexible, and therefore deformable, but the design should also have a large effective bandwidth. Unfortunately, membrane mechanics do not allow for such a combination of traits within a design. However, by augmenting our system with a fluid-filled cavity modeled like a distributed spring and damper, we will be able to modify the response of the membrane mirror such that it can still remain flexible while maintaining a large, effective bandwidth.

In this chapter, we will first discuss the dynamics of the membrane mirror, and demonstrate experimentally and through a numerical example how a fluid-filled cavity behaving like a spring and damper can be easily introduced into a membrane mirror design to attenuate the response of the membrane mirror over a large bandwidth. Next, we will discuss the response of the cavity to thermal effects from possible orbital pathways. Finally, we will conclude by summarizing the main contributions of this chapter.

7.2 Two Approaches for Modeling Cavities and Membranes

In this section, we will first look at Morse's model (1936) for a membrane vibrating over an enclosed cavity. The results of Morse's analysis show an aerodynamic spring effect that enters into the equation of motion due to the cavity on the backside of the membrane. However, the results of Morse's analysis demonstrate that only the symmetric normal modes of a circular membrane are positively affected by the presence of the cavity; the anti-symmetric normal modes are unaffected. In a second approach, we will model the back cavity as a distributed damper and spring, and demonstrate a broadband reduction in vibration levels to significantly increase the effective bandwidth of the membrane mirror without increasing the pre-stress in the membrane.

7.2.1 Morse's Kettledrum Model

As derived previously in Chapter 4, the equation of motion governing the transverse dynamics of a membrane under tension is given by:

$$\sigma \frac{\partial^2 \eta}{\partial t^2} = T \nabla^2 \eta \,. \tag{7.1}$$

If the membrane is vibrating over an enclosed cavity, then an excess pressure will develop on the backside of the membrane (within the volume of the cavity). This excess pressure enters into the equation of motion as a pressure term acting on each differential element, namely:

$$\sigma \frac{\partial^2 \eta}{\partial t^2} = T \nabla^2 \eta - p \,. \tag{7.2}$$

A diagram of this interaction is shown in Figure 7.1.

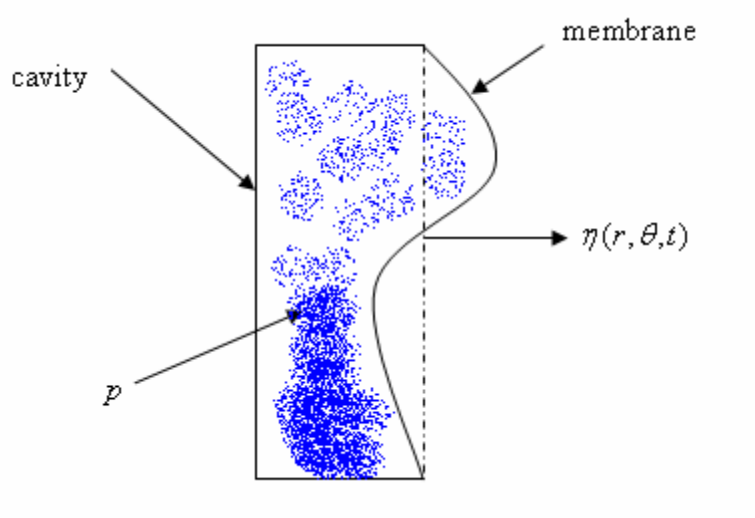

Figure 7.1. Diagram of a membrane vibrating over an enclosed cavity.

If the cavity is hermetically sealed, then the problem is analyzed as a kettledrum. Morse (1936) solved the kettledrum problem by assuming the gas is compressed and expanded adiabatically. A brief outline of his solution procedure is as follows. As the membrane undergoes vibration, the surface is displaced by some distance from the equilibrium position as described by the function $\eta(r, \theta, t)$. The volume of the air within the cylinder of radius a is changed by

$$\int_0^{2\pi} \int_0^a \eta \, r \, dr \, d\theta \,. \tag{7.3}$$

If we assume that the alterations in pressure within the cylinder are rapid enough to be considered adiabatic changes, then the excess pressure inside the cylinder is given by:

$$p = -\left(\frac{\rho_o c_a^2}{V_o}\right)\int_0^{2\pi}\int_0^a \eta\, r\, dr\, d\theta\,, \tag{7.4}$$

where ρ_o is the equilibrium density of the air, c_a is the speed of sound waves in air (at equilibrium temperature and density), and V_o is the equilibrium air volume of the cylinder (Morse, 1936). The excess pressure is given with a negative sign because it is always opposing the net displacement of the membrane. The integral term appearing in Equation 7.4 is a means of expressing the average displacement of the membrane, and has been used in the design of microphones (a concept to be discussed in more detail shortly).

The solution to plugging Equation 7.4 into the equation of motion given by 7.2 was carried out by Morse. The result of his analysis is that the air within the cavity acts as an aerodynamic spring, consequently increasing the resonant frequencies of the system. However, due to the integral term of Equation 7.4 in polar coordinates, not all of the frequencies of vibration are increased due to the presence of the kettledrum effect. Only the symmetric normal modes of vibration of the circular membrane are affected. Consequently, designing a membrane mirror with a sealed cavity would not be as beneficial as one might think since the bandwidth of the system would still be limited by the first anti-symmetric mode of vibration.

As an example of Morse's theory, Table 7.1 provides the resonant frequencies of the membrane based on a particular cavity geometry at atmospheric pressure. As shown, the "kettledrum effect" acts like an aerodynamic spring and increases the frequencies of symmetric membrane mode shapes considerably, especially at small cavity depths. In the numeric example, the tension is 5.6 N/m, the radius of the membrane is 7 cm, the membrane material is 12 μm Mylar (with a density of 1290 kg/m^3), the depth of the cavity is 5 mm, and the speed of sound is assumed to be 343 m/s. Figure 7.2 shows the first three symmetric mode shapes of an ideal membrane, while Figure 7.3 shows the first three symmetric mode shapes of a membrane backed by a shallow cavity, as predicted by Morse's theory.

Table 7.1. Comparison of symmetric, resonant frequencies of an ideal membrane and a kettledrum based on Morse's theory.

Frequency (Hz)	$\mathbf{f_{01}}$	$\mathbf{f_{02}}$	$\mathbf{f_{03}}$
Membrane	100	230	361
Morse's Kettledrum	214	351	485

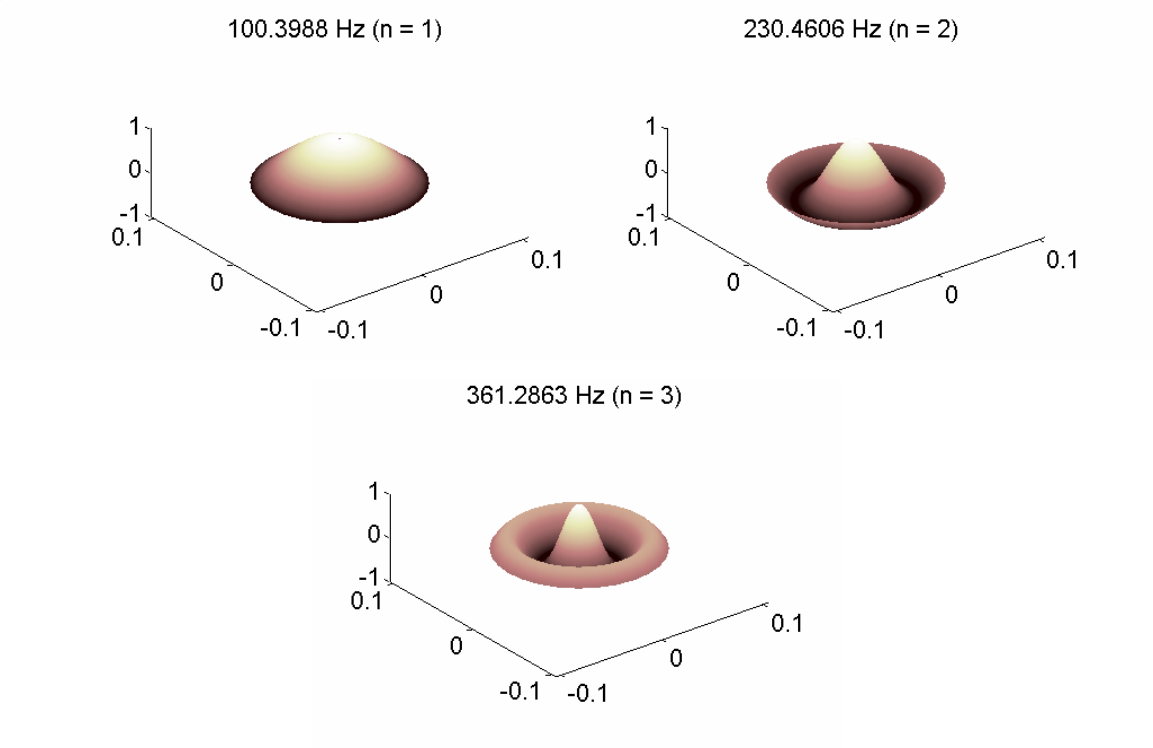

Figure 7.2. Mode shapes of an ideal membrane.

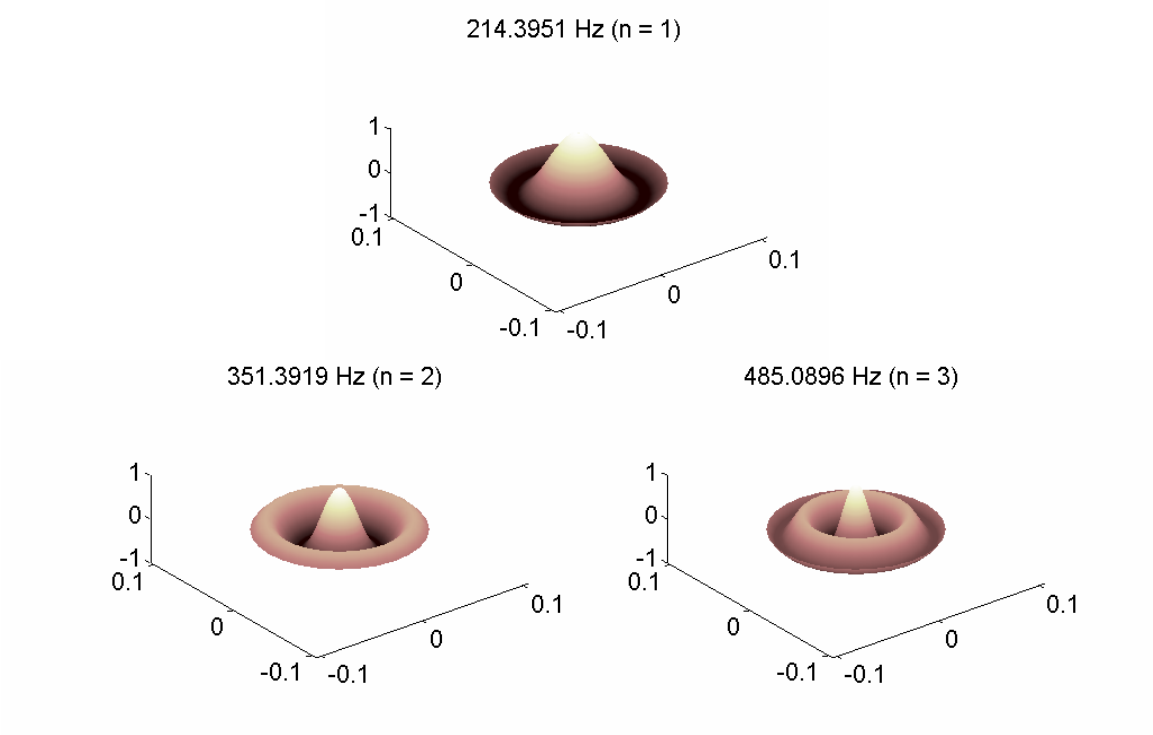

Figure 7.3. First three symmetric mode shapes of a cavity-backed membrane, as predicted by Morse's theory.

7.2.2 Passive Vibration Attenuation using Fluid Viscosity

The idea of incorporating a passive form of damping with membrane mirrors has only been addressed in the literature by two references: Grosso and Yellin (1977), the landmark paper from which most of the present work is based, and Takami and Iye (1994). Grosso and Yellin mention viscous air damping as the source of damping for their membrane mirror, and quote as their reference "[5] M. J. E. Golay (private correspondence)" (Grosso and Yellin, 1977)—a difficult reference to track down at the library. They do not try to model the effect of viscous air damping in their presented work. The following discussion addresses specifically the benefit of incorporating a fluid-filled cavity behind a membrane mirror.

First, though, a note on condenser microphone designs. A condenser microphone consists of a diaphragm held in tension over a capacitive plate with a small gap between

the two. In most condenser microphone designs, a potential is created across the gap between the thin plate and diaphragm. As sound waves excite the diaphragm, the electrical capacitance between the diaphragm and thin plate generates an output voltage that is proportional to the average displacement of the diaphragm. This signal is then amplified. The goal of designing an effective condenser microphone is to make the diaphragm as uniformly sensitive as possible to incident sound waves, and the presence of a properly designed back cavity (usually modeled as a damped Helmholtz resonator) enhances the effective bandwidth of the microphone.

For the current application of a membrane optic, the idea is proposed to augment a back cavity on the membrane filled with air (or another gas) like that of a condenser microphone. However, as opposed to making the membrane sensitive to incident waves, we wish to design it such that it is insensitive to dynamic disturbances. In essence, we wish to design a "terrible" condenser microphone, and in doing so, create a desirable membrane optic that has an increased effective bandwidth.

Suppose the cavity depth of Figure 7.1 was significantly smaller than the radius of the membrane lens, so that the ratio $\frac{L}{r} << 1$. In this case, we can approximate the response of the air within the cavity as a distribution of springs and dampers acting on each differential element of the membrane. Figure 7.4 shows this concept.

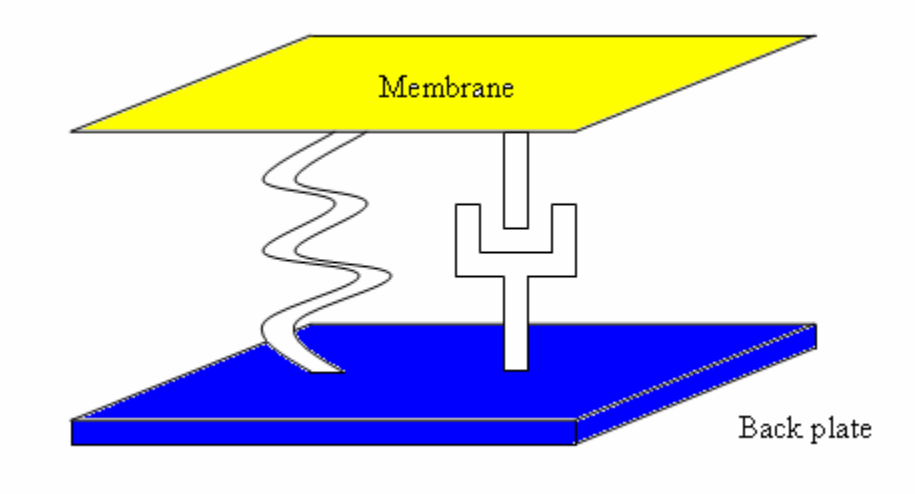

Figure 7.4. For shallow cavity depths, the air on the backside of the membrane acts like a spring and damper on each differential element.

Although it is an over simplification of the true physics of the system, the use of spring and damper elements between the membrane and back plate will provide a convenient means for understanding the behavior of the combined system.

As the membrane begins to vibrate when subject to some external disturbance, a backpressure develops between the cavity and the backside of the membrane (as shown in Figure 7.1). The backpressure then excites the air within the cavity. The dynamics of the air, if modeled as a spring and damper acting locally on each differential element of the membrane, can be described by:

$$D\frac{d\eta}{dt} + K\eta = p\,. \tag{7.5}$$

Plugging 7.5 into 7.1 yields

$$\sigma\frac{\partial^2\eta}{\partial t^2} = T\nabla^2\eta - D\frac{d\eta}{dt} - K\eta\,. \tag{7.6}$$

From Equation 7.6, we see that the effective stiffness of the combined system has increased based on the local stiffness of the entrapped air, but more importantly, a viscous damping term proportional to the local velocity of the membrane has been introduced into the equation of motion. Consequently, based on the structural design of the cavity, we can tailor the effective damping in the coupled system. As no active components have been introduced into the system, the addition of a fluid-filled back cavity is, in effect, a passive vibration attenuator for the membrane optic.

7.3 Experimental Demonstration of the Distributed, Damped Cavity Effect

An experiment was conducted to demonstrate the distributed spring and damper effects that a small cavity can introduce into the dynamics of a membrane optic or aperture. The experiment consisted of a circular Mylar membrane stretched taut over a 14 cm (5.5") diameter hole cut from a piece of acrylic. The membrane was pres-stressed uniformly using a knitting hoop—an easy and inexpensive way to achieve near-uniform stress in a circular membrane. The hoop was then glued using Super Seal caulk to the acrylic sheet, forming an airtight seal.

To excite the membrane, a small piece of magnetic material was placed on the surface of the Mylar membrane. An electromagnet was then situated in front of the magnetic material, and the interaction between the magnetic forces of the magnetic material and the electromagnet was used to dynamically excite the membrane. For further details on using the electromagnet as an excitation actuator for dynamic testing, see section 6.3.1. A photograph of the experimental setup is shown in Figure 7.5.

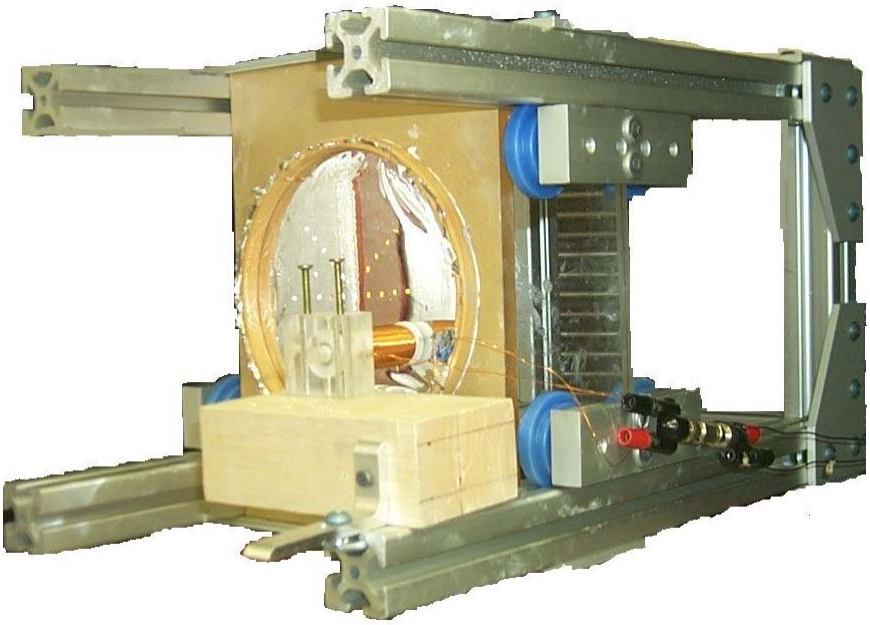

Figure 7.5. Photograph of the Mylar membrane and the electromagnet used as the excitation source to dynamically test the structure.

The response of the Mylar membrane was measured using a Polytec laser vibrometer. The velocity signal was filtered using an Ithaco high pass filter set to 80 Hz. The filter eliminated low-frequency noise from the measured signal and drastically improved the signal quality of all the measured responses. Also, 80 Hz was well below the first measurable dynamics of the membrane, so the response data was unaffected by the filter. The test stand, as shown in Figure 7.5, was designed such that the cavity depth could be adjusted using a lead screw. The linear bearings in the test stand in combination with the lead screw allowed for precise movements of the back plate. An exploded view of the test stand is shown in Figure 7.6.

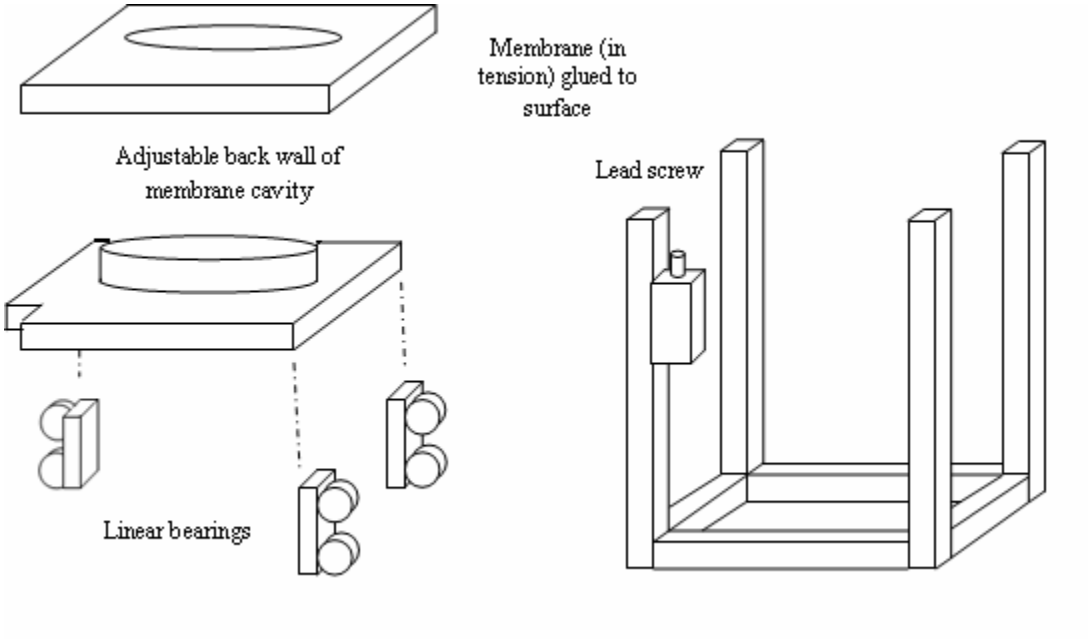

Figure 7.6. Diagram of the test stand used to adjust the cavity depth behind the membrane.

7.3.1 Cavity Effects as a Function of Depth

The test stand and membrane were mounted within the Tenney Environmental vacuum chamber. A series of tests were performed at three cavity depths: 1.0, 3.4, and 5.9 mm. Figure 7.7 depicts the locations of velocity measurements taken throughout the series of experiments. Dynamic response data was collected at a pressure of 10 Torr. The cavity depth was set first to 5.9 mm, then 3.4 mm, and finally 1.0 mm. To demonstrate the distributed spring and damper effects the air-filled cavity has on the dynamics of the membrane, Figures 7.8 – 7.12 show waterfall plots of the response of the membrane as a function of frequency and cavity depth at 10 Torr at five points within the domain of the membrane.

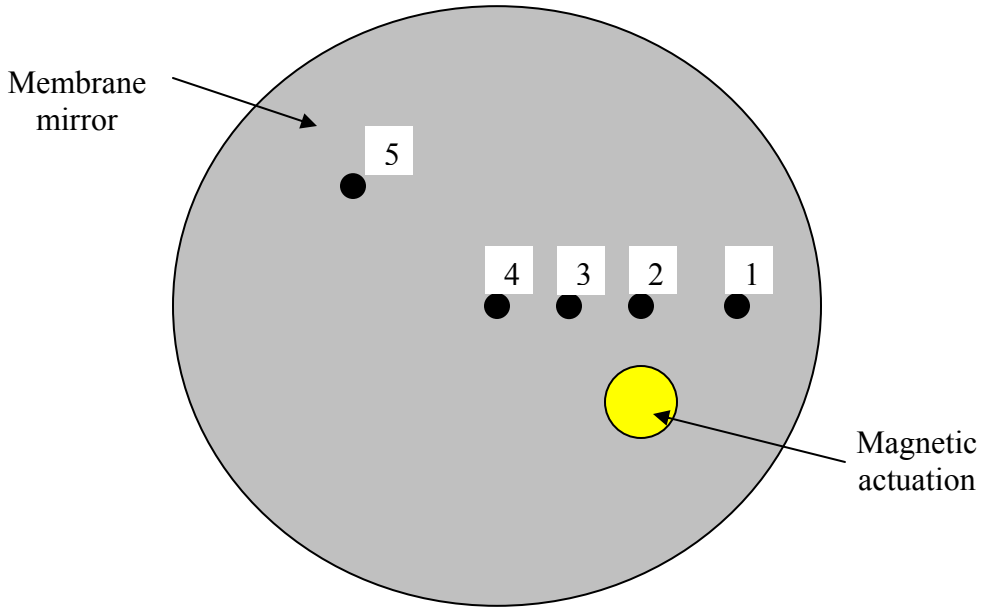

Figure 7.7. Diagram of velocity measurement locations on the surface of the membrane mirror.

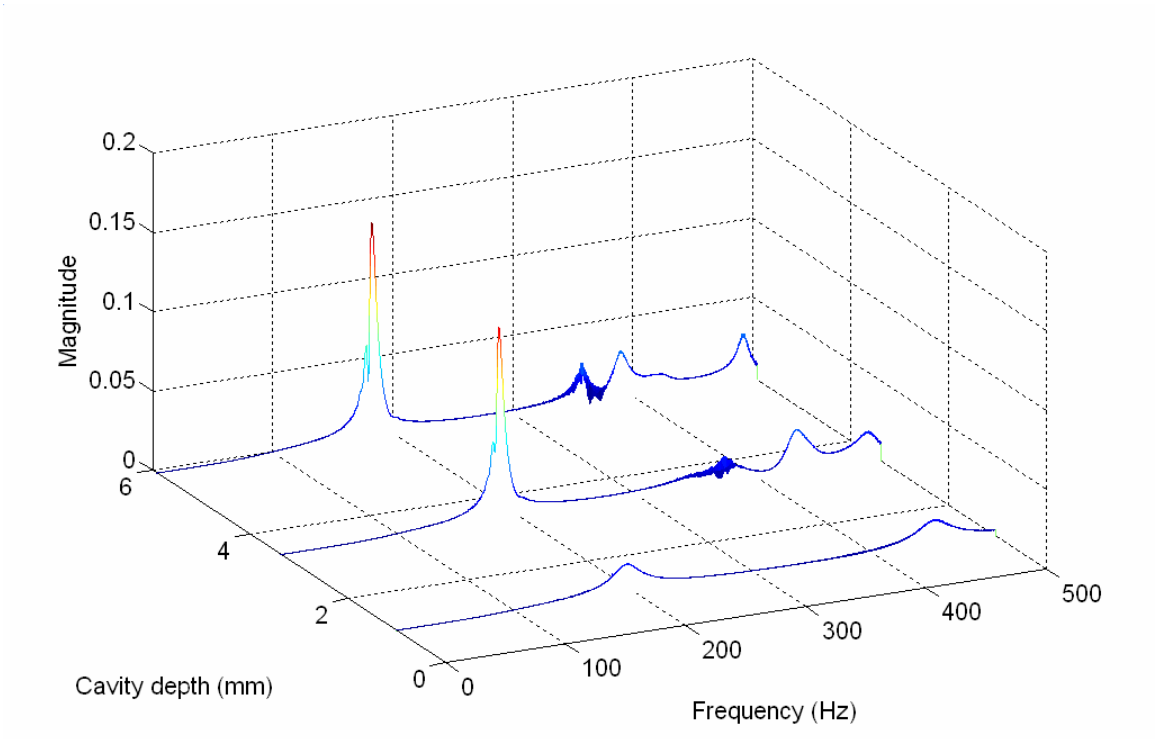

Figure 7.8. Frequency response function of the Mylar membrane at point 1 at 10 Torr. Note the enhanced, damped dynamics caused by the air-filled cavity.

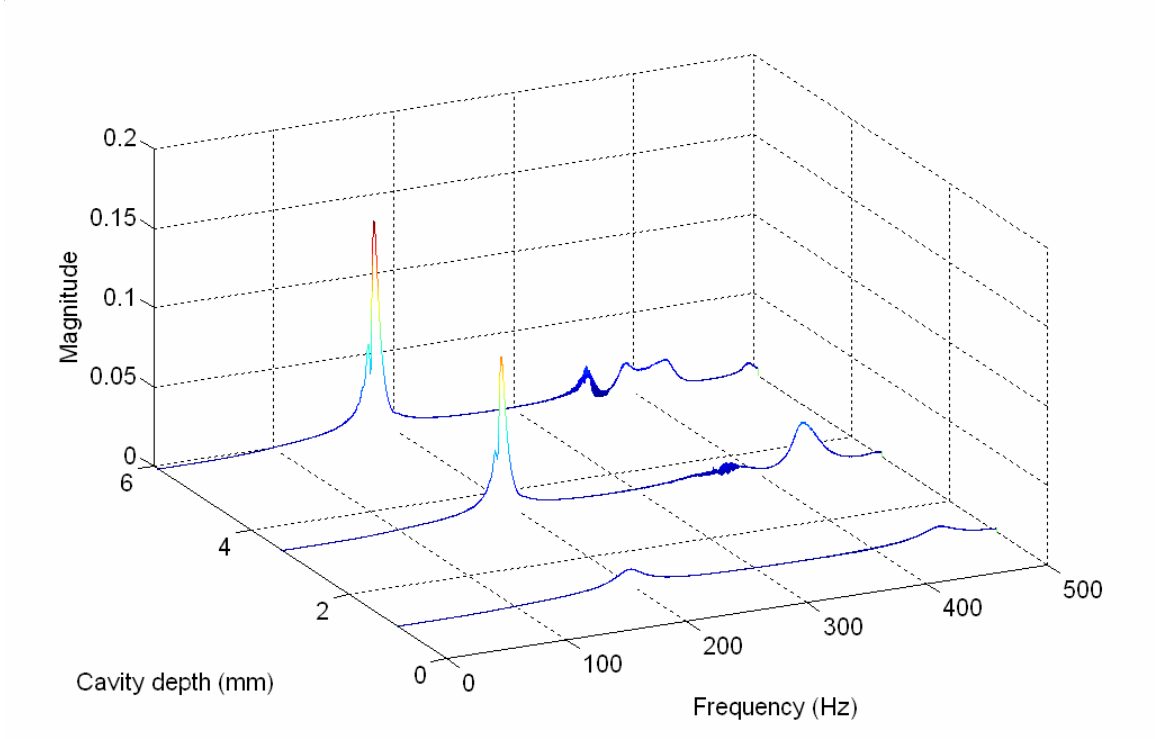

Figure 7.9. Frequency response function of the Mylar membrane at point 2 at 10 Torr. Note the enhanced, damped dynamics caused by the air-filled cavity.

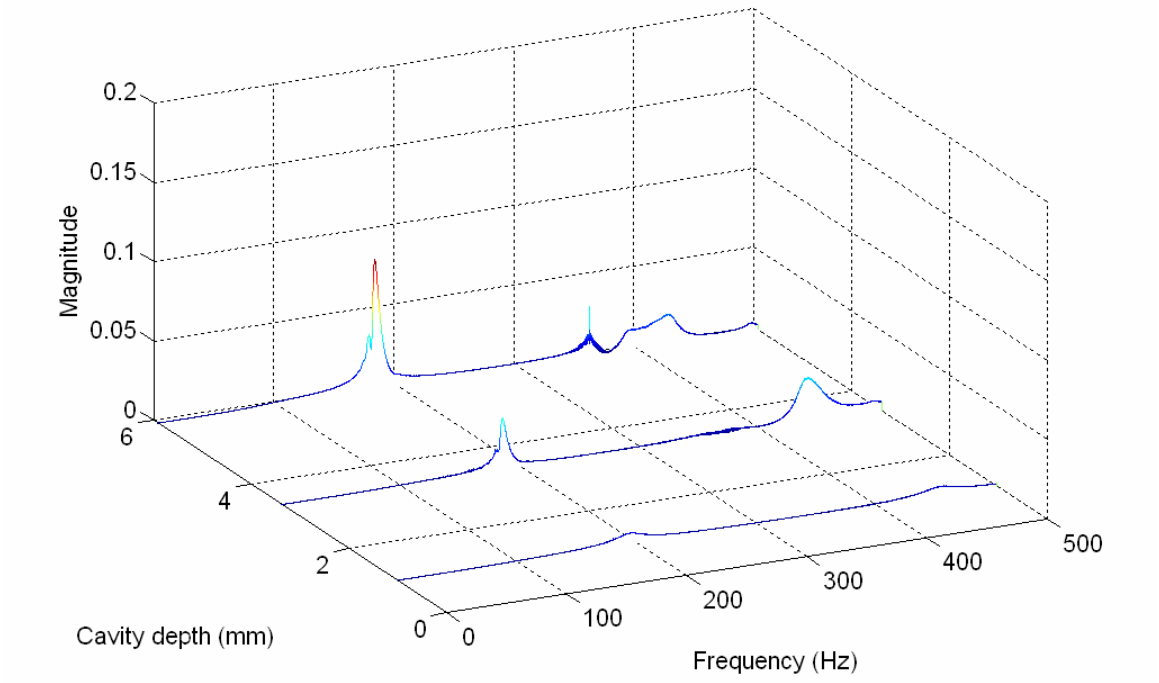

Figure 7.10. Frequency response function of the Mylar membrane at point 3 at 10 Torr. Note the enhanced, damped dynamics caused by the air-filled cavity.

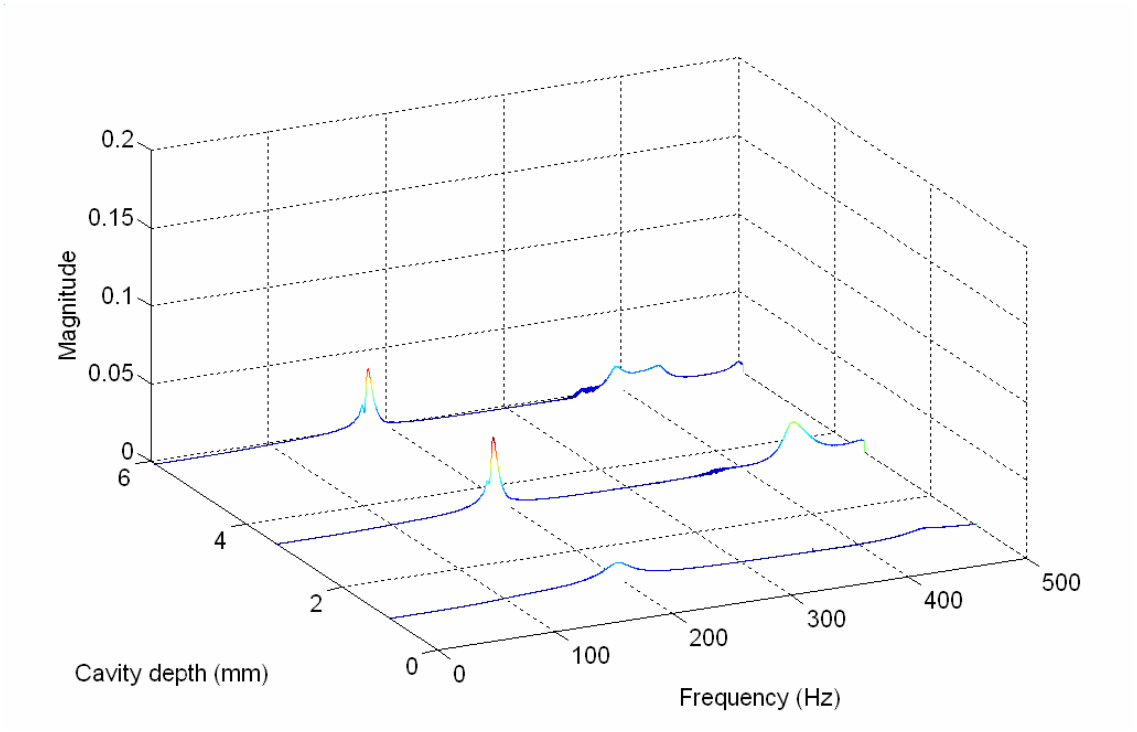

Figure 7.11. Frequency response function of the Mylar membrane at point 4 at 10 Torr. Note the enhanced, damped dynamics caused by the air-filled cavity.

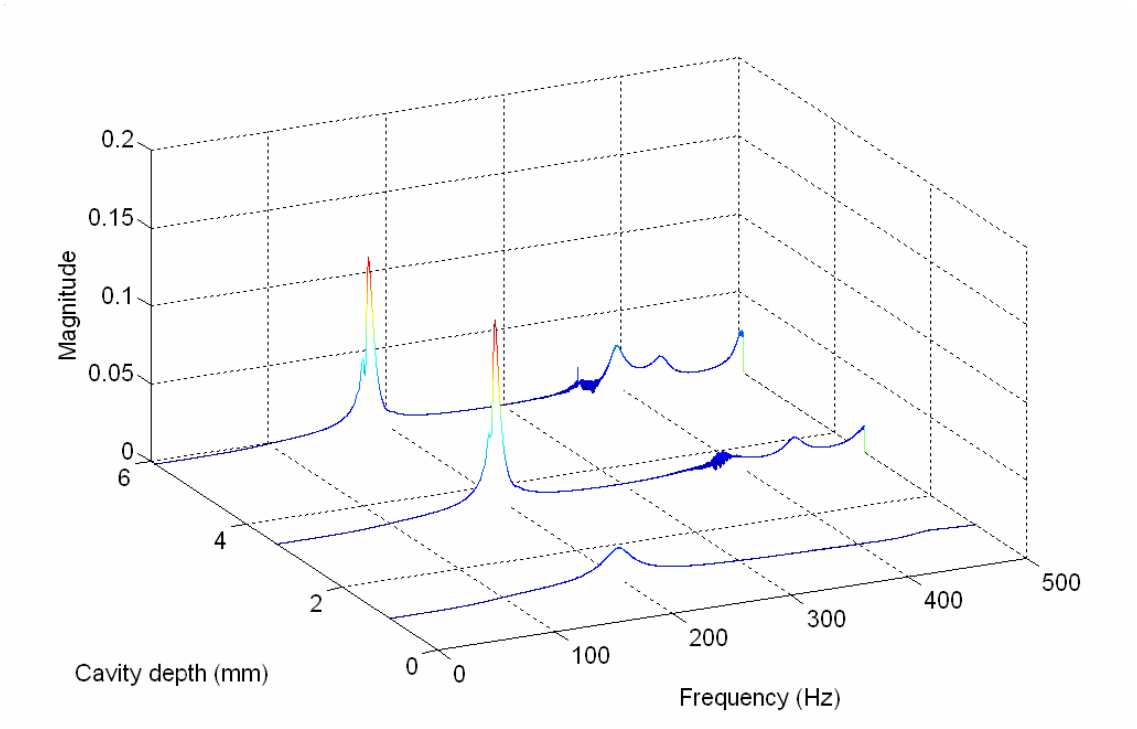

Figure 7.12. Frequency response function of the Mylar membrane at point 5 at 10 Torr. Note the enhanced, damped dynamics caused by the air-filled cavity.

As the back plate of the cavity is brought closer to the membrane, the response of the membrane demonstrates vibration attenuation, higher levels of damping, and an air spring effect. Figure 7.13 compares a bode plot of the membrane response measured at the center location of the membrane at 10 Torr with a cavity depth of 1.0 mm to the response of the membrane at the same location and chamber pressure but without a back cavity.

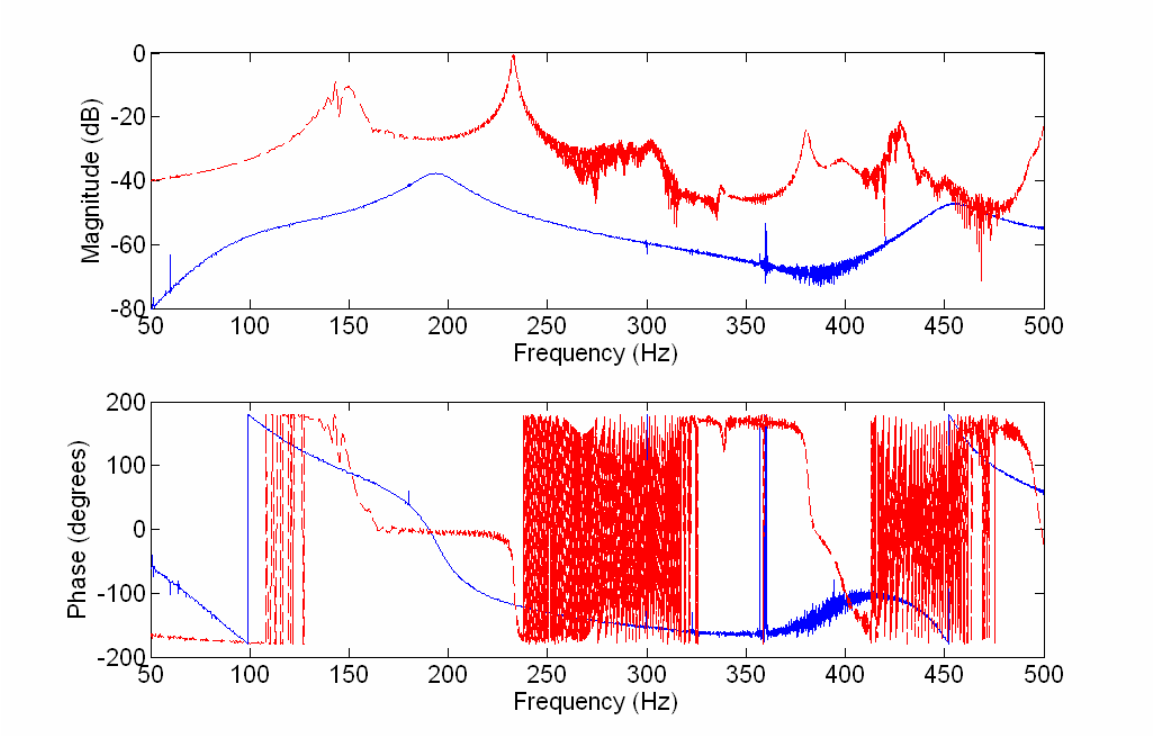

Figure 7.13. Bode plot of the membrane's dynamic response measured at point 4 on the membrane at a pressure of 10 Torr with a cavity depth of 1.0 mm (solid line) and without a cavity (dashed line).

7.3.2 Discussion of Experimental Results

The introduction of a shallow back cavity to the membrane produces desirable dynamics. The response of the membrane mirror becomes more heavily damped, increases all of the resonant frequencies, and attenuates the levels of vibration considerably. For example, as shown in Figure 7.13, without the presence of a back cavity, the membrane's primary resonant response, as excited by the electromagnet, is at 144 and 148 Hz (a split mode pair of the axisymmetric structure caused by the material discontinuity of the attached

magnet). With the introduction of a 1.0 mm cavity, the primary resonant response is shifted to 194 Hz and demonstrates a 28 dB reduction in vibration. The second resonant frequency of the membrane is at 232 Hz, but with the 1.0 mm cavity, the second resonant response occurs at 455 Hz at a vibration level 47 dB *less* than the original membrane configuration.

The primary conclusions that can be drawn from the experimental data collected is that the air trapped within the shallow cavity behind the membrane acts as both a distributed spring and a distributed damper. These results are in agreement with Morse (1936), who provides a short commentary on condenser microphone design where the back cavity is extremely close to the membrane mirror. He states, "…when the backing plate is very close [to the membrane]…, it is somewhat better to assume that the friction is localized, that each portion of air reacts only against that portion of membrane nearest to it" (Morse, 1936). He goes on to say that for a real system with trapped air acting as both a spring and damper, "[The] effect is to increase all of the frequencies of resonance, to lengthen the effective frequency range of the microphone, and to diminish the amplitude of response" (Morse, 1936).

We will use the equation of motion modeling the air as a distributed spring and damper as a means of simulating the response of the coupled system. Although the trapped air may be better modeled using more complicated mechanisms for stiffness and damping, the present model will serve its purpose for gathering further insight into the coupled response of the enclosed air volume and membrane.

7.4 Simulation of the Membrane-Cavity System

Next, we wish to model the dynamics of the membrane and the air within the cavity behaving like a distributed spring and damper. To do so, we will again use finite elements, as we have in previous chapters. For the numerical study, we will first have to define the weak form of Equation 7.6. Following a similar procedure as outlined in the previous two chapters, the finite element approximation to the weak form of Equation 7.6 is defined as

$$\begin{bmatrix} M_1 & 0 \\ 0 & M_2 \end{bmatrix}\begin{bmatrix} \vec{d} \\ \vec{v} \end{bmatrix}_t = \begin{bmatrix} 0 & M_1 \\ -K_1 - K_2 & -C \end{bmatrix}\begin{bmatrix} \vec{d} \\ \vec{v} \end{bmatrix}, \tag{7.7}$$

where

$$\begin{aligned} \left[M_1\right]_{i,j=1}^{N} &= \int_{\Omega} \phi_i \phi_j \, d\Omega \\ \left[M_2\right]_{i,j=1}^{N} &= \int_{\Omega} \sigma \phi_i \phi_j \, d\Omega \\ \left[K_1\right]_{i,j=1}^{N} &= \int_{\Omega} T\left[\left(\phi_i\right)_x \left(\phi_j\right)_x + \left(\phi_i\right)_y \left(\phi_j\right)_y\right] d\Omega \, . \\ \left[K_2\right]_{i,j=1}^{N} &= \int_{\Omega} K \phi_i \phi_j \, d\Omega \\ \left[C\right]_{i,j=1}^{N} &= \int_{\Omega} \left(D + \gamma\right) \phi_i \phi_j \, d\Omega \end{aligned} \tag{7.8}$$

In Equation7.8, T is the applied tensile load, σ is the areal density of the membrane, γ is a viscous damping term impeding the response of the membrane as it vibrates in air, K is the spring stiffness of the entrapped air, and D is the distributed damping parameter caused by the entrapped air.

The simulation will be performed on a square membrane, as the finite element analysis tool used throughout this work was designed for Cartesian coordinates and not polar coordinates. However, by creating a square membrane of equal surface area to that of the experimental setup, the phenomenological response of the simulated system can be compared to the experiment. Further, the presence of degenerate modes within a circular membrane is also a feature of a square membrane. Figure 7.14 shows the finite element mesh of the square membrane. For the model, we need to define some constants. Table 7.2 provides the necessary geometric and material properties used in the model.

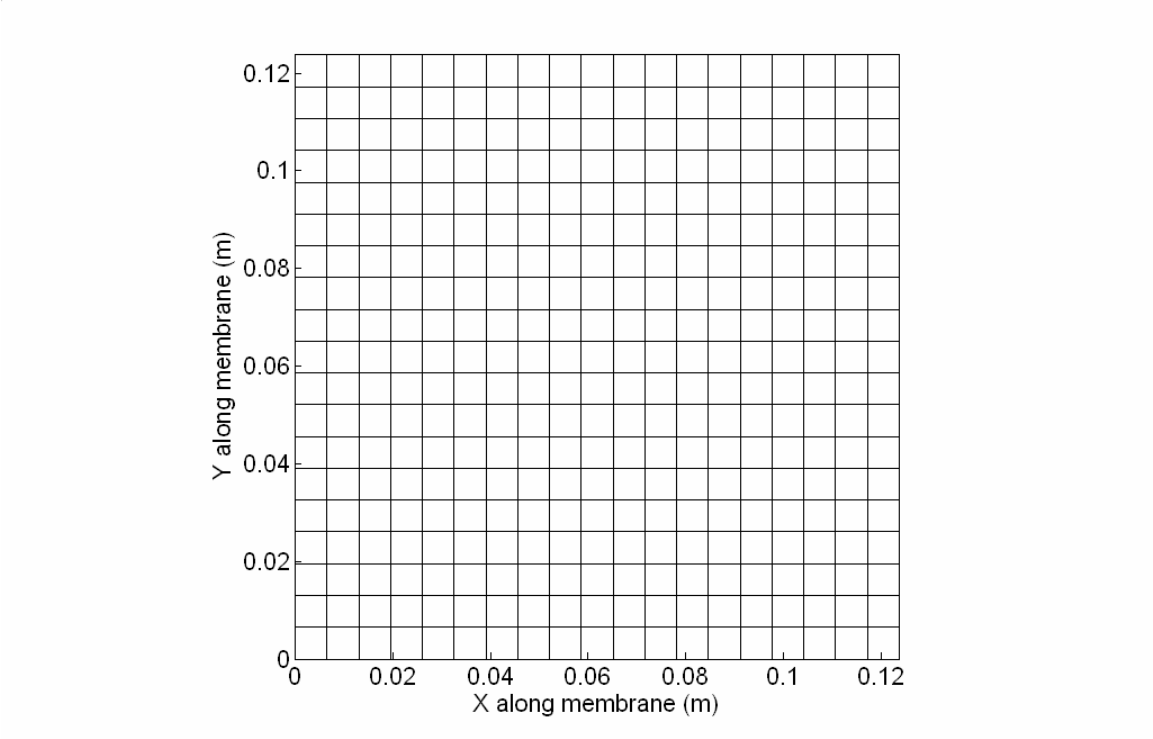

Figure 7.14. Finite element mesh of the square membrane used for numerical simulation.

Table 7.2. Geometric and material properties of the simulated square membrane.

Description	Value
Mylar density	1390 kg / m^3
Mylar thickness	12 μm
Tensile Loading	5.3 N / m
Density of air (room temperature and pressure)	1.293 kg / m^3
Depth of cavity	1.0 mm
Viscosity of air	.0000182 N s / m^2
Surface area	0.0153 m^2
Length of membrane edge	12.4 cm

The average velocity response of the membrane over a small, discrete area can be simulated. Similarly, a discrete force can be introduced into the developed model to simulate the interaction of the magnetic fields used for exciting the membrane. Of key importance to Equation 7.8 is knowing the magnitudes of the variables *K* and *D* induced by the enclosed air. The spring stiffness of the air, *K*, is a function of internal pressure, cavity dimension, and the speed of sound. As a starting point, let's assume that the stiffness term is proportional to Morse's (1936) proposed kettledrum term, namely,

$$K = \frac{\rho_0 c_a^2 A}{V_0}, \tag{7.9}$$

where ρ_0 is the density of the fluid, c_a is the speed of sound, V_0 is the equilibrium volume of the cavity, and A is the area of the membrane. Plugging in nominal values into Equation 7.9, we get a stiffness coefficient of $K = 2.1 \times 10^6\ N/m^3$. However, simulation of a stiffness value of this magnitude created a shift in the primary resonant frequency far too great to be considered realistic (>300%). From the simulations, a stiffness parameter value of $K = 10000$ was chosen as it shifted the primary resonance 36%. This percentage shift is similar to what was demonstrated experimentally. Figure 7.15 shows the simulated response of the membrane system at various stiffness values.

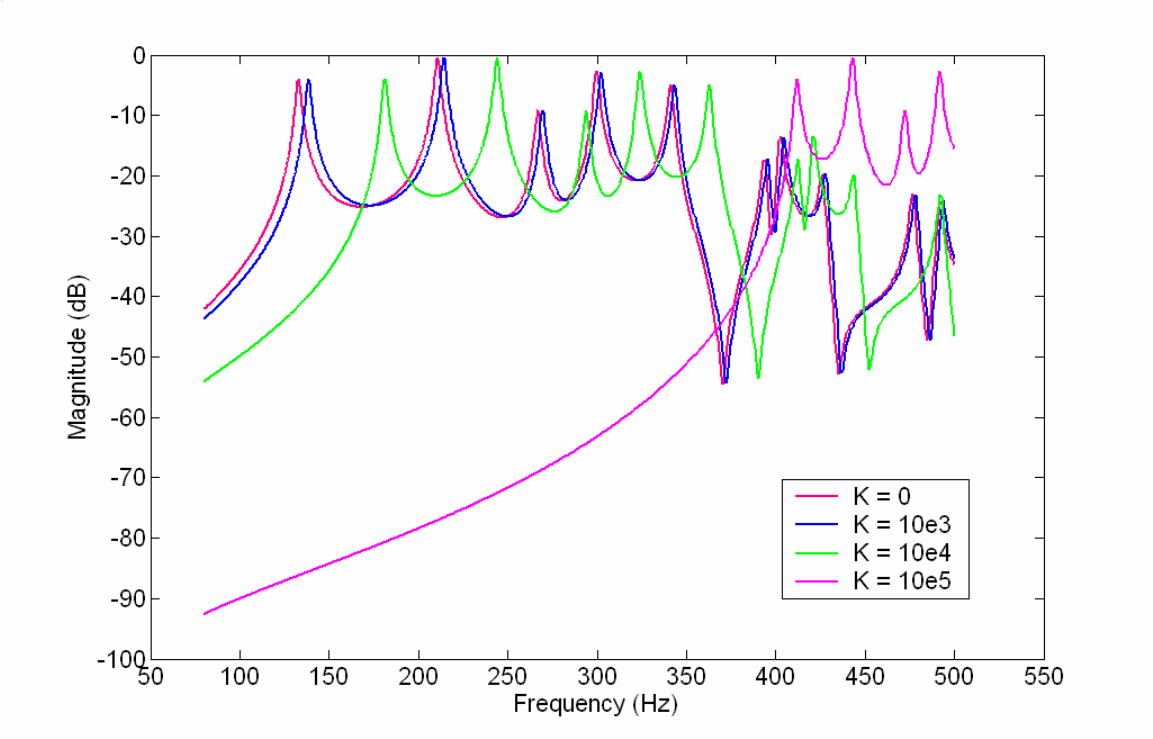

Figure 7.15. Simulated velocity response of a square membrane using different magnitudes for the stiffness value, *K*.

Estimation of the damping value, *D*, does not have an easily derived formula. However, based on the experimentally determined data, we can simulate the response of our square membrane and see what magnitude of *D* attenuates the vibration levels on the order of 30 dB (as this was shown experimentally). Figure 7.16 shows the effect of increased values of damping, *D*, on the dynamics of the system.

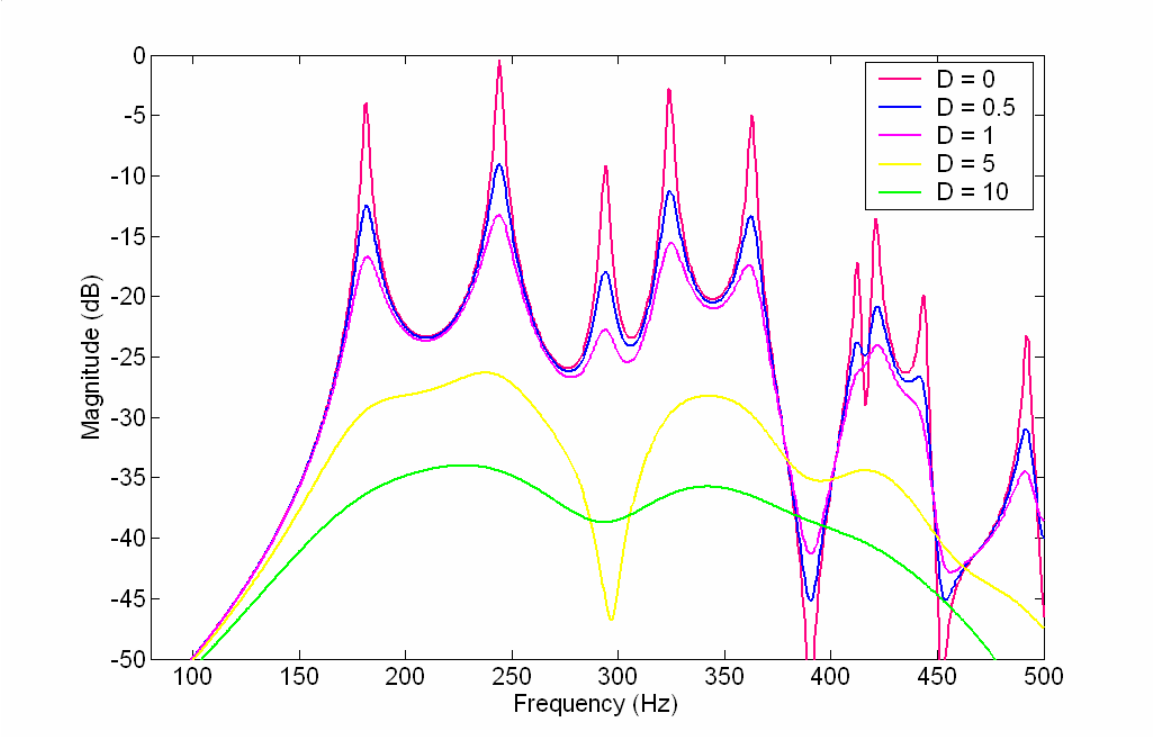

Figure 7.16. Simulated velocity response of a square membrane using different magnitudes for the damping value, *D*.

Note from Figure 7.16 that for a damping value $D = 10$, the response of the membrane emulates high damping (as expected), but that the response of the membrane between resonant peaks is more uniform and at a significantly lower level of vibration compared to the undamped case. The filling in of the anti-resonances is characteristic of increased damping within the system, and such a trend has also been identified in the experimental data. The "smoothing" out of the membrane's dynamics over a large bandwidth is a desirable effect, as it means the response of the membrane will be uniform to dynamic disturbances. Figure 7.17 compares the original response of the square membrane to the response of the membrane with a cavity acting as a distributed spring and damper.

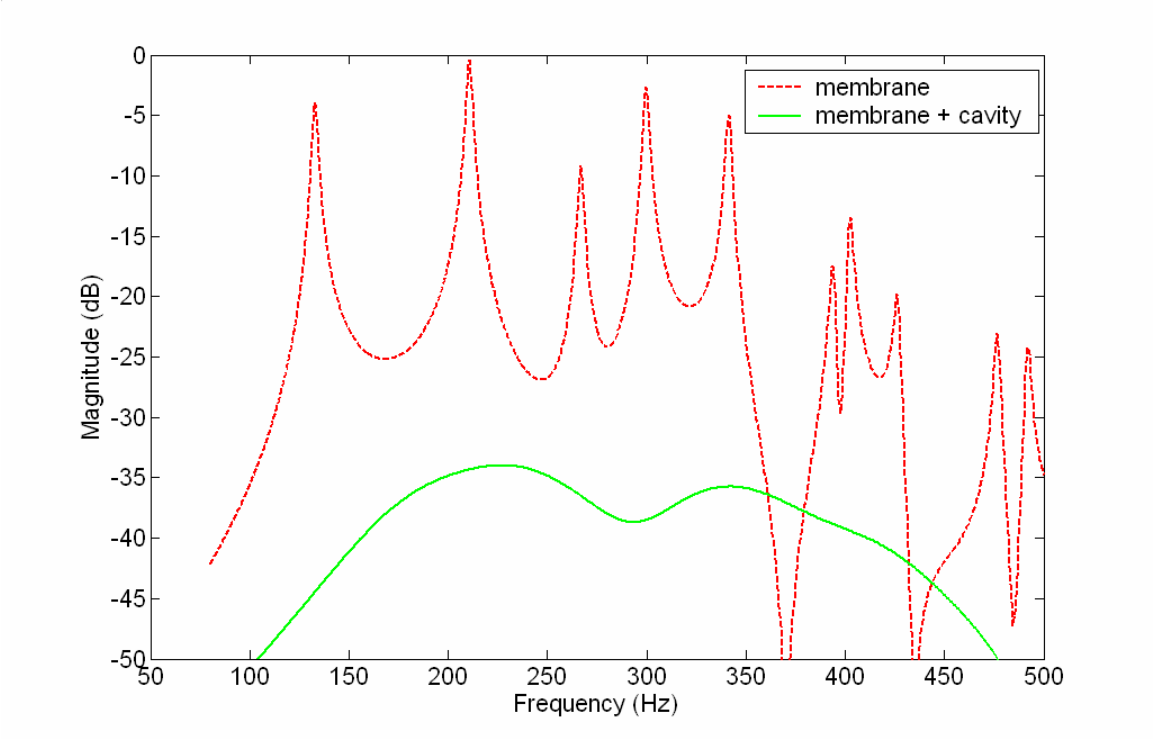

Figure 7.17. Simulated response of a square membrane with and without a back cavity (*K = 10000, D = 10*).

The response of the membrane augmented with a back cavity is a means of passively dissipating energy within the system to attenuate detrimental levels of vibration. However, a key criticism of this technology is that it relies on the use of an internal pressure to positively affect the system dynamics. In space, the membrane mirror system will be subject to direct solar radiation and possibly the Earth's shadow while on-orbit. These drastic temperature changes could possibly wreck havoc with the internal pressure of the membrane optic. To address this issue, we will perform a worst case thermal analysis to understand the consequences of such environmental conditions on the internal pressure.

7.5 Back-of-the-Envelope Thermal Analysis—A Hedgepeth Approach

In lines with the simple, back-of-the-envelope approach suggested by Hedgepeth (1981), we will look at a method of calculating the temperature extremes experienced by a membrane mirror satellite. There are two temperature scenarios that the membrane can

experience while operating on-orbit. The high temperature scenario is when it is in direct sunlight and direct Earth IR emission. In the cold temperature scenario, the satellite is completely in the Earth's shadow and receives just the IR emission from the Earth. A diagram of these two extreme cases is shown in Figure 7.18.

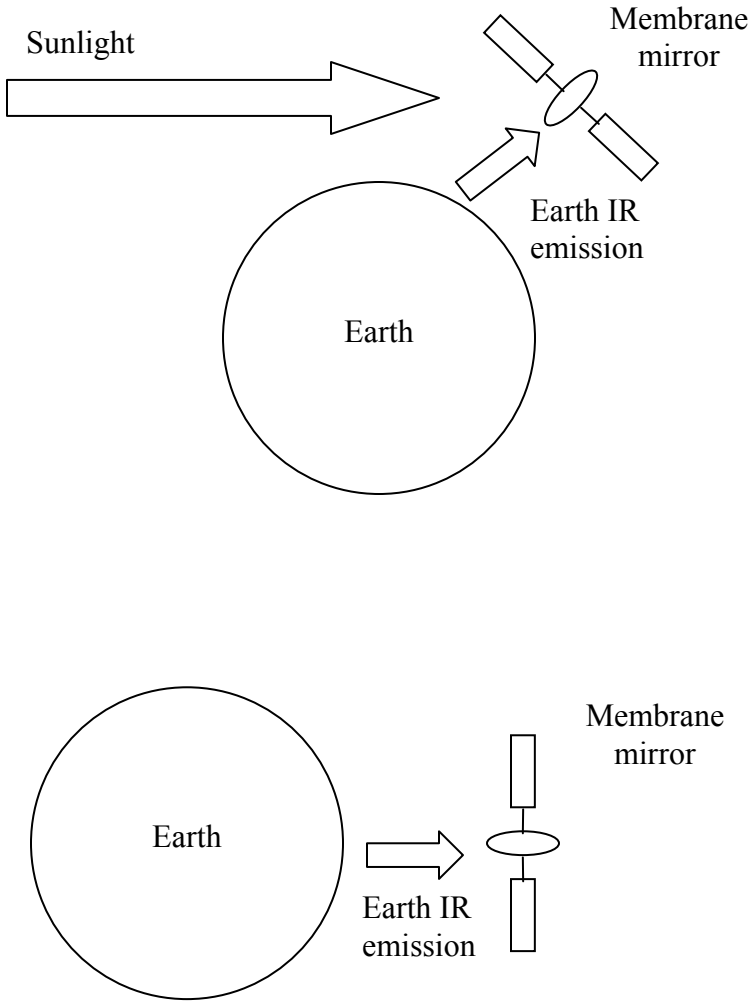

Figure 7.18. Extreme temperatures that the membrane mirror could encounter while on-orbit, from the hottest (top) to the coldest (bottom) cases.

In performing this heat transfer analysis, we will assume that the membrane mirror behaves like a flat plate adiabatically insulated on the backside. In making this assumption, we are assuming that the gas trapped within the cavity behind the membrane does not affect the energy absorption of the membrane. Although this is not the case for

the true system, such an assumption will provide extreme hot and cold cases for the analysis. Further, it will be assumed that the gas comes to thermal equilibrium in the two extreme cases. Based on these assumptions, the equilibrium temperature of the thin plate can be solved for by the equation (Wertz and Larson, 1999):

$$T = \left[\frac{(G_s + q_i)\alpha}{\varepsilon\sigma} \right]^{1/4}, \tag{7.9}$$

where G_s is the solar constant (1418 W / m^2), q_i is the Earth IR emission (237 ± 21 W / m^2), α is the absorptivity of Mylar (0.17), ε is the emissivity of Mylar (0.76), and σ is the Stefan-Boltzmann's constant (5.67051 x 10^{-8} W / (m^2 K^4)). Using these nominal values, the resultant equilibrium temperatures are given by:

$$\begin{aligned} T_{hot} &= 12^o C \\ T_{cold} &= -102^o C \end{aligned}. \tag{7.10}$$

The extreme values calculated in Equation 7.10 demonstrate an immediate, critical need for thermal management within the system (and also demonstrate why Mylar should not be used as a space optic). Using the ideal gas law, assuming that the pressure within the cavity at 12°C was 10 Torr, then at the other extreme, when the satellite is in the Earth's shadow, we have

$$\frac{P_1 V_1}{T_1} = \frac{P_2 V_2}{T_2} \Rightarrow P_2 = \frac{P_1 T_2}{T_1} = \frac{(10\,Torr)(171\,K)}{285\,K} = 6\,Torr\,. \tag{7.11}$$

Proper thermal management will be a necessity of the membrane – cavity system for two reasons. Firstly, from a structural perspective, a uniform temperature distribution across the structure will ensure mechanical equilibrium and prevent optical distortion induced by thermal expansion or contraction. Secondly, thermal management will also ensure that the pressure within the cavity does not change dramatically, as the dynamics of the membrane mirror are susceptible to large pressure variations.

A number of thermal management systems are available, ranging from passive to active solutions. The type of solution required will be determined by the mission requirements and designated orbital path of the membrane mirror. At this time, such requirements are still undefined. As an example of thermal management, consider the X-ray Multi-mirror Mission spacecraft. The X-ray Multi-mirror Mission spacecraft (Fortescue, Startk, and Swinerd, 2003), subsequently renamed *Newton*, is an advanced X-ray observatory in a highly elliptical orbit to avoid influence from the Earth's trapped radiation. Throughout its 48 hour orbit, the temperature of the critical X-ray telescope components must be maintained at 20^{o}C, with an allowable variation of 2^{o}C. *Newton*'s design incorporated heaters controlled by a mirror thermal control unit and has been quite successful. More stringent temperature requirements are also possible, such as fluctuations on the order of 0.5^{o}C, but with the consequence of additional mass and required power from active thermal systems.

Since the membrane-cavity system requires low pressure values (10 Torr has been demonstrated as an effective pressure for enhanced, damped dynamics in the current chapter), the pressure to the cavity could be easily maintained using a pressure regulator in conjunction with thermal management. Consequently, although the design is susceptible to temperature fluctuations, proper thermal management combined with an additional supply pressure could easily alleviate thermal issues. As an added benefit, the pressure regulator could be used in an adaptive optics scheme, as will be discussed in the next chapter.

7.6 Chapter Summary

In this chapter, we experimentally investigated the effect of placing a shallow cavity on the backside of a membrane mirror. In analyzing the resulting system dynamics, it was demonstrated that the response of the membrane could be enhanced from two perspectives. Firstly, the enclosed cavity of air provides a local stiffness reaction, and consequently increases all of the resonant frequencies of the system. Secondly, the viscosity of the fluid within the small gap between the membrane and cavity wall

provides a significant source of damping on the membrane dynamics. The drastic increase in system damping creates a more uniform response over a large bandwidth at significantly attenuated vibration levels. Consequently, the response of the membrane is like a poorly designed condenser microphone—it is rather insensitive to incident pressure waves or disturbances. The membrane's lack of sensitivity over a large bandwidth translates into either a membrane optic or radar aperture that remains in focus despite the introduction of dynamic disturbances. In effect, the back cavity provides a distributed, passive stiffness and damping mechanism to enhance the bandwidth of the system.

The distributed stiffness and damping mechanism was demonstrated numerically on a square membrane Mylar sample. The stiffness term was found iteratively based (initially) on the kettledrum stiffness term suggested by Morse (1936). Then, a damping value was found through numerical investigation to produce equivalent vibration attenuation as seen in the experimental structure. Vibration attenuation levels on the order of 30 and 50 dB were demonstrated both experimentally and numerically. Relating the design of the cavity to the actual spring and damping mechanisms provided by the enclosed cavity will be a topic discussed in the future works section.

Finally, a back-of-the-envelope calculation (similar to the types of calculations performed by Hedgepeth (1981)) was performed for predicting the temperature extremes experienced by a Mylar membrane mirror. The results of the calculations showed an incredible temperature swing, from -102^{o}C to 12^{o}C. By using a gas within the cavity, like air, the pressure within the cavity will be susceptible to temperature fluctuations. Using the ideal gas law, and assuming that the enclosed air acts ideally, such a pressure fluctuation translates into a pressure swing from 6 Torr to 10 Torr. However, through proper thermal management, possibly by active means, and by providing a pressure regulator for the cavity, such temperature effects can be mitigated.

In the next chapter, we will explore the use of pressure within the membrane cavity as a means of accomplishing adaptive (or deformable) optics. The enhanced dynamics of the membrane as demonstrated in this chapter avoided increasing the applied pre-stress

within the membrane. Consequently, the membrane surface can remain relatively flexible and, as we will show numerically, can be used as a deformable mirror for adaptive optics.